

On Proximity of 4/7 Solid Phase of ^3He Adsorbed on Graphite -Origin of Specific-Heat Anomalies in Hole-Doped Density-Ordered Solid-

Shinji WATANABE and Masatoshi IMADA

Department of Applied Physics, University of Tokyo, Hongo 7-3-1, Bunkyo-ku, Tokyo, 113-8656, Japan

We theoretically study the stability of the solidified 2nd-layer ^3He at 4/7 of the 1st-layer density adsorbed on graphite, which exhibits quantum spin liquid. We construct a lattice model for the 2nd-layer ^3He by taking account of density fluctuations on the 3rd layer together by employing the refined configuration recently found by path integral Monte Carlo simulations. When holes are doped into the 4/7 solid, within the mean-field approximation, the density-ordered fluid emerges. The evolution of hole pockets offers a unified explanation for the measured doping and temperature dependences of specific-heat anomalies. We argue that differentiation in momentum space is a key to understanding the physics and accounts for multiscale thermodynamic anomalies in the mono- and double-layered ^3He systems beyond the mean-field level.

KEYWORDS: quantum spin liquid, ^3He , 4/7 phase, density-ordered fluid, hole pocket, zero point vacancy

Layered ^3He systems adsorbed on graphite offer unique playgrounds as an ideal prototype of strongly correlated Fermion systems in purely two dimensions. At the 4/7 density of the 2nd-layer ^3He relative to the 1st-layer density, ^3He atoms are solidified to form a triangular lattice, which is referred to as the 4/7 phase.¹ The 4/7 phase has attracted much attention recently, since specific heat² and susceptibility measurements down to 10 μK ³ have suggested the emergence of a gapless quantum spin liquid.

Theoretically, the multiple-spin-exchange model⁴ has been used for the analysis,^{5,6} which, however, has left fundamental questions about the 4/7 phase: (1) How to realize the gapless ground state? (2) How to explain the large saturation field of about 10 T⁷? To resolve these issues, we have pointed out the importance of density fluctuations between the 2nd and 3rd layers.⁸ By constructing a lattice model to describe the 4/7 solid phase, we have shown that strong density fluctuations indeed stabilize a gapless quantum spin liquid, which can be regarded as that caused essentially by the same mechanism found in the Hubbard model.⁹⁻¹² Furthermore, the density fluctuation accounts for the enhanced saturation field as observed.⁸

In this letter, we report our analysis of the stability of the 4/7 phase on the basis of the lattice model, taking account of density fluctuations. The model is derived from a refined configuration of the 2nd-layer ^3He recently revealed by path-integral Monte Carlo (PIMC) simulations.¹³ Our mean-field (MF) results show that a density-ordered fluid emerges when holes are doped into the 4/7 phase and that the evolution of the hole pockets explains measured specific-heat anomalies. Our model gives a unified explanation of unusual temperature and doping dependences of specific heat over a range from the 4/7 solid phase to the uniform-fluid phase at low densities. We also discuss the validity of the present picture beyond the MF approximation and possible relevance to the specific-heat anomalies measured recently in the double-layered ^3He system.¹⁴

Our analysis starts from the result of recent PIMC simulations,¹³ which have revealed a more stable configuration for the 4/7 phase than that first proposed by Elser^{1,15} as shown in Fig. 1(a). Here, the open circles represent the atoms on the 1st layer, and the shaded circles, the locations on the 2nd layer when solidified. If ^3He (^4He) atoms are adsorbed on the 1st layer, it forms a triangular lattice with the lattice constant $a=3.1826$ (3.1020) \AA at the saturation density $\rho_1=0.114$ (0.120) $\text{atom}/\text{\AA}^2$.¹

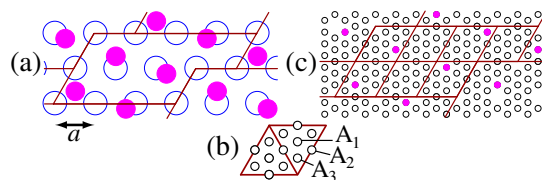


Fig. 1. (Color online) (a) Lattice structure of the 4/7 phase of ^3He shown by recent PIMC simulations.¹³ Both 1st-layer atoms (open circles) and 2nd-layer atoms (shaded circles) form triangular lattices in the solid phase. The area enclosed by the solid line represents the unit cell for the solid of the 2nd-layer atoms (see text). The lattice constant of the 1st layer is a . (b) Possible stable location of the 2nd-layer atoms are shown by circles on top of a $a \times a$ parallelogram constructed from the 4 neighboring 1st-layer atoms. (c) Structure of discretized lattice for the 2nd-layer model. Lattice points are shown by circles.

The location of the 2nd-layer atoms is in principle determined as stable points in continuum space under the periodic potential of the 1st layer. In the present treatment, we simplify the continuum by discretizing it with the largest possible number of lattice points kept as candidates of stable points in the solid. To illustrate discretization, we cut out from Fig. 1(a) a unit cell of the 1st layer, namely, a parallelogram whose corners are the locations on top of the neighboring 4 atoms on the 1st layer as in Fig. 1(b). Possible stable locations of ^3He atoms on the 2nd layer are points on top of (1) the cen-

ters of the 1st-layer triangle (A_1), (2) the midpoint of two-neighboring 1st-layer atoms (A_2), and (3) a nearby point of the 1st-layer atom (A_3). Therefore, we employ totally 11 points as discretized lattice points in a parallelogram, shown as circles in Fig. 1(b). Since a unit cell in Fig. 1(a) contains 7 parallelograms, it contains 77 lattice points in total, as illustrated as circles in Fig. 1(c). Now the 4/7 solid phase is regarded as a regular alignment of 4 atoms on 77 available lattice points in the unit cell shown in Fig. 1(c).

For inter-helium interaction, we employ the Lennard-Jones potential $V_{LJ}(r) = 4\epsilon \left[(\sigma/r)^{12} - (\sigma/r)^6 \right]$, where $\epsilon = 10.2$ K and $\sigma = 2.56$ Å.¹⁶ A more refined Aziz potential is expected to give similar results under this discretization. The interaction between ^3He atoms on the 2nd layer is given by $H_V = \sum_{ij} V_{ij} n_i n_j$ (n_i is the number operator of a Fermion on the i -th site) with V_{ij} taken from the spatial dependence of $V_{LJ}(r)$ on the lattice points. In the actual ^3He system, the chemical potential of the 3rd layer is estimated to be 16 K higher than that of the 2nd layer.¹⁷ ^3He atoms may fluctuate into the 3rd layer over this chemical potential difference and it is signaled by a peak of the specific heat at $T \sim 1$ K.^{18–20} To take account of this density fluctuation, we here mimic the allowed occupation on the 3rd layer by introducing a simple finite cutoff V_{cutoff} for V_{ij} within the same form of Hamiltonian: When $V_{LJ}(r_{ij})$ for $r_{ij} \equiv |\mathbf{r}_i - \mathbf{r}_j|$ exceeds V_{cutoff} , we take $V_{ij} = V_{\text{cutoff}}$, otherwise $V_{ij} = V_{LJ}(r_{ij})$. This allows us to take account of the qualitative but essential part of the possible occupation on the 3rd layer by atoms overcoming V_{cutoff} .

We consider the spinless-Fermion model on the lattice $H = H_K + H_V$ where the kinetic energy is given by $H_K = -\sum_{\langle ij \rangle} (t_{ij} c_i^\dagger c_j + \text{H.C.})$. We ignore the effects of corrugation potential from the 1st layer for the moment and discuss it later. By using the unit-cell index s and the site index l in the unit cell, we have $\mathbf{r}_i = \mathbf{r}_s + \mathbf{r}_l$. After the Fourier transform, $c_i = c_{s,l} = \sum_{\mathbf{k}} c_{\mathbf{k},l} e^{i\mathbf{k}\cdot\mathbf{r}_s} / \sqrt{N_u}$, the MF approximation with the diagonal order parameter $\langle n_{\mathbf{k},l} \rangle$ leads to

$$H_V \sim H_V^{\text{MF}} = \frac{1}{N_u} \sum_{l,m=1}^{77} \sum_{s'} V^{lm}(s') \sum_{\mathbf{k},\mathbf{p}} \left[\langle n_{\mathbf{k},l} \rangle n_{\mathbf{p},m} - \frac{1}{2} \langle n_{\mathbf{k},l} \rangle \langle n_{\mathbf{p},m} \rangle \right],$$

where the inter-atom interaction is expressed as $V_{ij} = V_{st}^{lm} = V^{lm}(s')$ with $\mathbf{r}_{s'} = \mathbf{r}_s - \mathbf{r}_t$. Then, we have the MF Hamiltonian $H_{\text{MF}} = H_K + H_V^{\text{MF}}$. By diagonalizing the 77×77 Hamiltonian matrix for each \mathbf{k} , we obtain the energy bands $H_{\text{MF}} = \sum_{\mathbf{k}} \sum_{l=1}^{77} E_l(\mathbf{k}) c_{\mathbf{k},l}^\dagger c_{\mathbf{k},l}$.

For the kinetic energy, several choices of t_{ij} are examined. As noted in ref. 8, if t_0 is determined so as to reproduce the total kinetic energy E_K^{PIMC} , the main result below, measured in the unit of K, is quite insensitive to the choice of t_{ij} . Hence, we here show the results for $t_{ij} = t_0$ for the ij pairs up to the shortest-19th r_{ij} , i.e., for $|r_{ij}| \leq 2a$. The interaction V_{ij} is taken for $r_{ij} \leq 2a$, since the longer r_{ij} part is ineffective.⁸ The recent PIMC simulation estimates the kinetic energy of the 2nd-layer ^3He in the 4/7 phase as $E_K^{\text{PIMC}} = 14$ K (17 K) for the

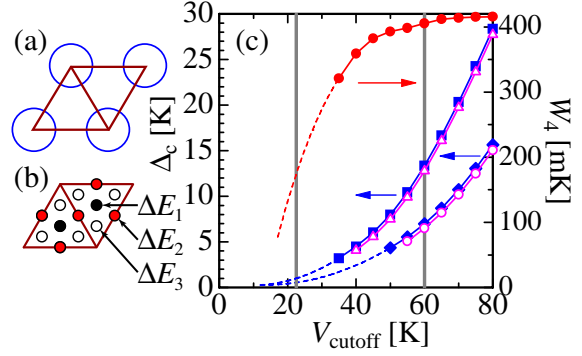


Fig. 2. (Color online) (a) Parallelogram formed by 4-neighbouring 1st-layer atoms. (b) The sites for 2nd-layer atoms in the parallelogram under corrugation potentials ΔE_1 (solid circle), ΔE_2 (shaded circle) and ΔE_3 (open circle). (c) V_{cutoff} dependence of the “charge gap” Δ_c for $\Delta E_1 = \Delta E_2 = \Delta E_3 = 0$ (filled square) and for $\Delta E_1 = -3.0$ K, $\Delta E_2 = -1.5$ K and $\Delta E_3 = 0$ K (open triangle) in the $^3\text{He}/^4\text{He}/\text{Gr}$ system, and for $\Delta E_1 = \Delta E_2 = \Delta E_3 = 0$ (filled diamond) and for $\Delta E_1 = -3.0$ K, $\Delta E_2 = -1.5$ K and $\Delta E_3 = 0$ K (open circle) in the $^3\text{He}/^3\text{He}/\text{Gr}$ system. The bandwidth of the 4th band W_4 is illustrated for $\Delta E_1 = \Delta E_2 = \Delta E_3 = 0$ (filled circle) in the $^3\text{He}/^4\text{He}/\text{Gr}$ system. Shaded lines at $V_{\text{cutoff}} = 22.5$ K and 60 K are guides for the eyes (see text).

^4He (^3He) 1st layer.¹³ Thus, we evaluate t_0 by imposing the condition, $\sum_{\langle ij \rangle} t_0 (c_i^\dagger c_j + \text{H.C.}) / (4N_u) = E_K^{\text{PIMC}}$ as $t_0 = 413$ mK (502 mK) for the ^4He (^3He) 1st layer.

By solving the MF equations for H_{MF} , we have the solution of the $\sqrt{7} \times \sqrt{7}$ commensurate structure shown in Fig. 1(c) with opening the “charge gap” as shown by filled squares (diamonds) in Fig. 2(c) when ^4He (^3He) is adsorbed on the 1st layer. Here, the “charge gap” is defined by $\Delta_c \equiv E_5^{\text{min}}(\mathbf{k}) - E_4^{\text{max}}(\mathbf{k})$, where $E_l^\beta(\mathbf{k})$ denotes the minimum or maximum energy of the l -th band from the lowest. We show here the well-converged results for large Δ_c and the small- Δ_c region will be discussed later for detailed comparison with experiments. We now discuss the effects of corrugation potential. PIMC^{13,15} suggests that the 1st-layer atoms make the corrugation potential on the 2nd layer even within the discretized lattice points. It suggests $\Delta E_1 = -3.0$ K and $\Delta E_2 = -1.5$ K relative to ΔE_3 in the notation in Fig. 2(b). This effect merely shifts the Δ_c - V_{cutoff} line toward a larger V_{cutoff} , as shown by open triangles (circles) for the ^4He (^3He) 1st layer in Fig. 2(c). Hence, we show our results below for $\Delta E_1 = \Delta E_2 = \Delta E_3 = 0$ and for ^4He adsorbed on the 1st layer as a representative case.²¹ We note that Fig. 2(c) indicates that the 4/7 phase is more stable when ^4He is adsorbed on the 1st layer rather than the ^3He 1st layer.

The energy band $E_4(\mathbf{k})$ for $V_{\text{cutoff}} = 60$ K at $n_0 = 1$ with $n \equiv \sum_{l=1}^{77} \sum_{\mathbf{k}} n_{\mathbf{k},l} / (77N_u) = 4n_0/77$ and its contour plot in the folded Brillouin zone²² are shown in Figs. 3(a) and 3(b), respectively. When holes are doped into the 4/7 phase, in our MF results, the Fermi surface appears at the 4th band as hole pockets for $n_0 = 0.99$ (Fig. 3(c)) and $n_0 = 0.97$ (Fig. 3(d)) with the density order retained.

This evolution of hole pockets is reflected in thermodynamic quantities: As holes are doped into the 4/7 solid,

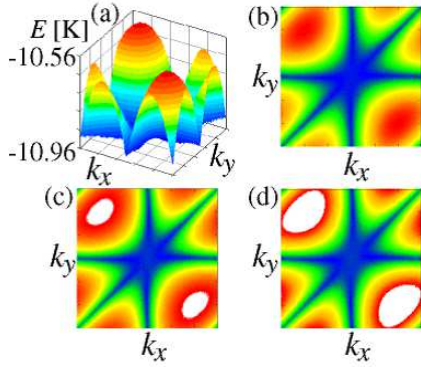


Fig. 3. (Color) (a) The 4th energy band in the folded Brillouin zone for $-\pi/\bar{a} \leq k_x \leq \pi/\bar{a}$ and $-\pi/\bar{a} \leq k_y \leq \pi/\bar{a}$ with $\bar{a} = 2\sqrt{7}a^{22}$ for $V_{\text{cutoff}} = 60$ K at $n_0 = 1$. Contour plot of the 4th band for (b) $n_0 = 1$, (c) $n_0 = 0.99$ and (d) $n_0 = 0.97$. Hole pockets are represented by white regions in (c) and (d).

a remarkable peak in the specific heat $C(T)$ develops at temperatures lower than the density-order transition temperature T_c , as shown in Fig. 4(a). At the same time, $C(T)$ at temperatures right below T_c decreases. The temperature T^* at which $C(T)$ has the highest peak for $T < T_c$ increases as n_0 decreases from 1, as indicated by arrows in Fig. 4(a). This tendency was actually observed in the past¹⁸ and recent²⁰ measurements: The λ -like anomaly at $T = T_c \sim 1$ K simultaneously with the hump at $T \sim 40$ mK in $C(T)$ observed for $n_0 = 0.96$ ¹⁸ and for $n_0 = 0.971$ ²⁰ is an indication of the coexisting density order and fluid. Since our model H is the spinless-Fermion model, the entropy per site $S(T)$ at the high-temperature limit is given by $k_B \ln 2$. When T decreases, $S(T)$ sharply drops at the density order T_c and the remaining entropy is released at $T \sim T^* < T_c$ as shown in Fig. 4(b).

In experiments, sharp decreases in $S(T)$ at much lower temperatures, i.e., $T \sim 0.2$ and 1 mK, are observed for $0.9 \lesssim n_0 \lesssim 1.02$,^{2,20} which result in a double peak in $C(T)$. This spin entropy is ignored in the present model. These sharp drops correspond to the release of the spin entropy at the energy scale of the spin exchange interaction J .²³ Under hole doping, the double peak at $T \sim 0.2$ and 1 mK is suppressed, whereas the hump $C(T^*)$ ²⁰ at 40 mK grows. This is naturally understood by the suppression of the density order simultaneously with an increase in the fluid contributions induced by doping. Actually, a double-peak structure in $C(T)$ around $T \sim J$ has been shown by our exact-diagonalization calculations⁸ for the density-ordered solid phase in a minimal lattice model, which was introduced to mimic the 4/7 solid.

To further clarify the origin of T^* , we calculated the density of states for $V_{\text{cutoff}} = 60$ K at $n_0 = 1$, as in Fig. 5(a). Since the energy gap opens in the 4/7 phase, $\Delta_c \sim 1$ K, the hump structure in $C(T)$ at $T \sim T^* \ll \Delta_c$ should arise from the 4th band. As holes are doped into the 4/7 phase, the chemical potential shifts to lower energies inside the 4th band, as shown by vertical lines in the inset of Fig. 5(a). In Fig. 4(a), we plot the energy difference between the top of the 4th band, $W_4^{\text{top}} \equiv E_4^{\text{max}}(\mathbf{k})$,

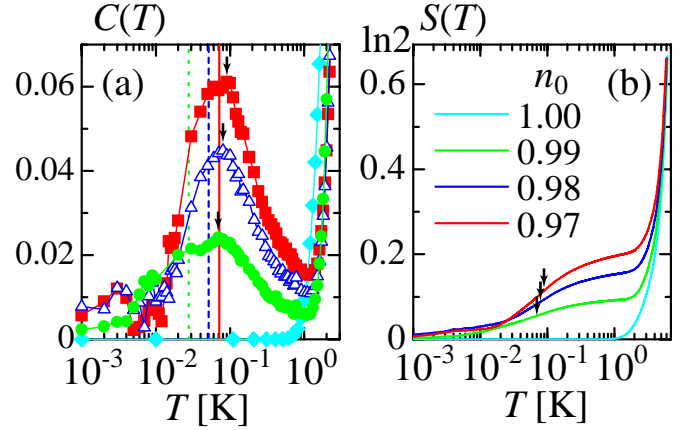


Fig. 4. (Color) (a) Specific heats for $n_0 = 1.0$ (light-blue diamond), 0.99 (green circle), 0.98 (blue open triangle), and 0.97 (red square) for $V_{\text{cutoff}} = 60$ K. $W_4^{\text{top}} - \mu = 0.99$ (green dotted line), 0.98 (blue dashed line), and 0.97 (red line). (b) Entropy per site for $n_0 = 1.0$ (light blue), 0.99 (green), 0.98 (blue), and 0.97 (red) for $V_{\text{cutoff}} = 60$ K. Arrows indicate the temperatures T^* at which $C(T)$ has the highest peak for $T < T_c$.

and the chemical potential μ , $W_4^{\text{top}} - \mu$, by vertical lines. We see that $W_4^{\text{top}} - \mu$ is located at the central position of the hump of $C(T)$ for each n_0 . This confirms that the characteristic energy of the fluid in the density-ordered-fluid phase expressed by $W_4^{\text{top}} - \mu$ corresponds to T^* . The filling dependences of T^* (open square) and $W_4^{\text{top}} - \mu$ (open diamond) are shown in Fig. 5(b).

To make a detailed comparison with experiments, we extrapolate the “charge gap” Δ_c by the least-squares fit of the data for $35 \text{ K} \leq V_{\text{cutoff}} \leq 45 \text{ K}$ assuming the form $\sum_{n=0}^2 a_n V_{\text{cutoff}}^n$,²⁴ which is shown by the dashed line in Fig. 2(c). We also extrapolate the width of the 4th band, $W_4 \equiv E_4^{\text{max}}(\mathbf{k}) - E_4^{\text{min}}(\mathbf{k})$ by the least-squares fit of the data for $35 \text{ K} \leq V_{\text{cutoff}} \leq 80 \text{ K}$ (filled circles in Fig. 2(c)) assuming the form $\sum_{n=0}^3 b_n V_{\text{cutoff}}^n$ and the result is represented by the dashed line in Fig. 2(c). Since the “charge gap” of the 4/7 phase is expected to be $\Delta_c \sim 1 \text{ K}$,^{8,18} the corresponding V_{cutoff} is estimated to be 22.5 K, which is not inconsistent with the chemical potential difference between the 2nd and 3rd layers, 16 K¹⁷ (the gray line in Fig. 2(c)). Then, W_4 at $V_{\text{cutoff}} = 22.5 \text{ K}$ is evaluated to be 174 mK. Since $W_4(V_{\text{cutoff}} = 22.5 \text{ K})/W_4(V_{\text{cutoff}} = 60 \text{ K}) \sim 0.43$, the density of states of the 4th band at $V_{\text{cutoff}} = 22.5 \text{ K}$ is inferred to be enhanced 1/0.43 times more than that at $V_{\text{cutoff}} = 60 \text{ K}$, as shown in the inset of Fig. 5(a). Then, $W_4^{\text{top}} - \mu$ and T^* at $V_{\text{cutoff}} = 22.5 \text{ K}$ are estimated to be 0.43 times smaller than those at $V_{\text{cutoff}} = 60 \text{ K}$, which are shown by filled diamonds and filled squares, respectively, in Fig. 5(b). The slope of the resultant T^* is evaluated to be $T^* \sim 400\delta \text{ mK}$ with $\delta \equiv 1 - n_0$, which is quite consistent with the experimental observation $T^* \sim 430\delta \text{ mK}$.²⁰ This analysis shows that T^* may be regarded as the effective bandwidth of the holes by quantum-mechanical zero-point motions in the solid, which substantiates the hypothesized idea of *zero-point vacancy*.^{20,25}

We note that the filling dependence of the entropy $S(T)$ for $T^* < T \ll T_c$ (for example, $S(T = 100 \text{ mK})$,

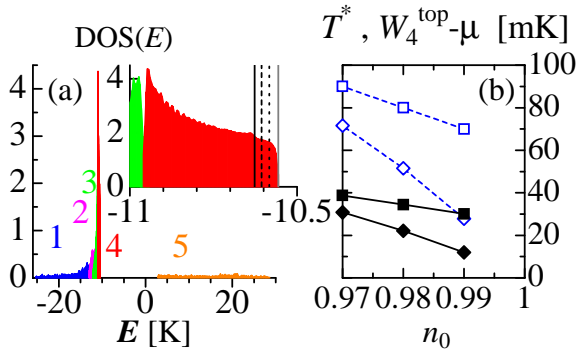


Fig. 5. (Color) (a) Density of states for the 1st (blue), 2nd (pink), 3rd (green), 4th (red), and 5th (light brown) bands for $V_{\text{cutoff}} = 60$ K at $n_0 = 1$. The inset shows the enlargement of the 4th band with W_4^{top} (gray line) and the chemical potential μ for $n_0 = 0.99$ (dotted line), 0.98 (dashed line), and 0.97 (solid line). (b) Filling n_0 dependence of T^* (square) and $W_4^{\text{top}} - \mu$ (diamond) for $V_{\text{cutoff}} = 60$ K (open symbols with dashed lines) and $V_{\text{cutoff}} = 22.5$ K (filled symbols with solid lines).

not shown) shows nearly the same n_0 dependence as $S = -n_0 \ln n_0 - (1 - n_0) \ln(1 - n_0)$, as experimentally observed.²⁰ This implies that the entropy for distributing $N\delta$ holes in the N -site system can be accounted for by the hole-pockets contribution in the density-ordered-fluid phase.

We note that a broad shoulder structure of $C(T)$ in the uniform fluid phase for $n_0 = 0.3$ (not shown) evolves into the $C(T^*)$ hump as n_0 increases, which finally shrinks toward $n_0 = 1$ as in Fig. 4(a). A similar $C(T)$ evolution was observed in the layered ^3He system on the two ^4He layers adsorbed on graphite by Neumann et al.¹⁴ when the ^3He density n increases and approaches $n_c = 9.9 \text{ nm}^{-2}$. Since $C(T)$ has common features in both systems,^{14,20} it is natural to interpret the intervening phase observed for $n_l < n < n_c$ with $n_l = 9.2 \text{ nm}^{-2}$ in ref. 14 as a density-ordered fluid stabilized near the density-ordered solid at $n = n_c$. This offers a clear and alternative interpretation of the sharp transition or crossover around $n = 9.2 \text{ nm}^{-2}$ in ref. 14.

The density-ordered fluid whose ground-state energy is lower than that of the uniform fluid, $E_{\text{DOF}}(n_0) < E_{\text{fluid}}^{\text{uni}}(n_0)$, is confirmed at least up to 7% hole doping for $V_{\text{cutoff}} = 60$ K. The poor convergence of the MF solution upon further doping prevents us from determining the accurate phase boundary.

Here, we also stress an alternative possibility, namely, the emergence of a uniform fluid phase with small Fermi surfaces when holes are doped into the density-ordered phase, even when fluctuations beyond the MF theory destroy the density order in the absence of spin order. The Fermi surface is defined by poles of the single-particle Green function $G(\mathbf{k}, \omega)$ at a frequency $\omega = 0$.²⁶ While $\text{Re}G$ changes its sign across a pole through $\pm\infty$, $\text{Re}G$ can also change the sign across a zero defined by $G = 0$. In the solid phase, only the zero surface exists in the \mathbf{k} space at $\omega = 0$ while only the poles exist at $\omega = 0$ for heavily doped uniform fluids. When holes are slightly doped, the reconstruction of $G(\mathbf{k}, \omega)$ yields the interference between

the zeros and the poles, which creates the resultant Fermi surface with the coexistence of zeros and poles. Since the interference has a significant \mathbf{k} dependence at $\omega = 0$, small Fermi pockets may appear after the truncation of the large Fermi surface²⁷ even when the density order is destroyed upon hole doping in the absence of the spin order. It is remarkable that not only doped Mott insulators but also doped density-order phases show such differentiation as observed in the 2D ^3He system. This differentiation in \mathbf{k} space can also be the origin of the peak (small cusp) at $T \sim J$ and the hump (peak) at $T \sim T^*$ in $C(T)$ for $n_0 < 1^{20}$ ($n < n_c$ ¹⁴), since the former and latter are attributed to the contributions from the truncated and remaining parts of the Fermi surface in \mathbf{k} space, respectively. A multiscale measurement of $C(T)$ ranging from 1 mK to 1 K is desired to resolve this issue in layered ^3He systems.

Acknowledgment

We thank Hiroshi Fukuyama for supplying us with experimental data and T. Takagi for showing us his PIMC data prior to publication with enlightening discussions on their analyses. This work is supported by Grants-in-Aid for Scientific Research on Priority Areas under grant numbers 17071003, 16076212 and 18740191 from MEXT, Japan.

- 1) V. Elser: Phys. Rev. Lett. **62** (1989) 2405.
- 2) K. Ishida, M. Morishita, K. Yawata, and H. Fukuyama: Phys. Rev. Lett. **79** (1997) 3451.
- 3) R. Masutomi, Y. Karaki, and H. Ishimoto: Phys. Rev. Lett. **92** (2004) 025301.
- 4) M. Roger, C. Bauerle, Yu. M. Munkov, A.-S. Chen, and H. Godfrin: Phys. Rev. Lett. **80** (1998) 1308.
- 5) G. Misguich, B. Bernu, C. Lhuillier, and C. Waldmann: Phys. Rev. Lett. **81** (1998) 1098.
- 6) T. Momoi, H. Sakamoto, and K. Kubo: Phys. Rev. B **59** (1999) 9491.
- 7) H. Nema, A. Yamaguchi, T. Hayakawa, and H. Ishimoto: unpublished.
- 8) S. Watanabe and M. Imada: J. Phys. Soc. Jpn. **76** (2007) 113603.
- 9) T. Kashima and M. Imada: J. Phys. Soc. Jpn. **70** (2001) 3052.
- 10) H. Morita, S. Watanabe, and M. Imada: J. Phys. Soc. Jpn. **71** (2002) 2109.
- 11) S. Watanabe: J. Phys. Soc. Jpn. **72** (2003) 2042.
- 12) T. Mizusaki and M. Imada: Phys. Rev. B **74** (2006) 014421.
- 13) T. Takagi: private communications.
- 14) M. Neumann, J. Nyéki, B. Cowan, and J. Saunders: Science **317** (2007) 1356.
- 15) F. F. Abraham, J. Q. Broughton, P. W. Leung, and V. Elser: Europhys. Lett. **12** (1990) 107.
- 16) J. de Boer and A. Michels: Physica **5** (1938) 945.
- 17) P. A. Whitlock, G. V. Chester, and B. Krishnamachari: Phys. Rev. B **58** (1998) 8704.
- 18) S. W. Van Sciver and O. E. Vilches: Phys. Rev. B **18** (1978) 285.
- 19) D. S. Greywall: Phys. Rev. B **41** (1990) 1842.
- 20) Y. Matsumoto, D. Tsuji, S. Murakawa, C. Bäuerle, H. Kambara, and H. Fukuyama: unpublished.
- 21) Similar temperature and doping dependences of specific heat appear for $\Delta E_1 = -3.0$ K, $\Delta E_2 = -1.5$ K and $\Delta E_3 = 0.0$ K, since nearly the same structure of the DOS around the top of the 4th band is realized in the MF framework, which is responsible for the low-temperature part of specific heat.
- 22) For simplicity of analysis, primitive translation vectors $\mathbf{R}_1 =$

$(5a, -\sqrt{3}a)$ and $\mathbf{R}_2 = (4a, 2\sqrt{3}a)$ are transformed as $\mathbf{R}_i^{(1)} = \hat{R}\mathbf{R}_i$, $\mathbf{R}_i^{(2)} = \hat{D}\mathbf{R}_i^{(1)}$ and $\mathbf{R}_i^{(3)} = \hat{S}\mathbf{R}_i^{(2)}$, where \hat{R} , \hat{D} and \hat{S} are given by

$$\begin{bmatrix} \cos \theta & -\sin \theta \\ \sin \theta & \cos \theta \end{bmatrix}, \begin{bmatrix} 1 & -R_{x2}^{(1)}/R_{y2}^{(1)} \\ 0 & 1 \end{bmatrix}, \begin{bmatrix} 1 & 0 \\ 0 & R_{x1}^{(2)}/R_{y2}^{(2)} \end{bmatrix},$$

respectively, with $\theta = -\arctan(R_{y1}/R_{x1})$. This $\mathbf{R}_i^{(3)}$ configuration makes the folded Brillouin zone a $2\pi/\bar{a}$ square with $\bar{a} = 2\sqrt{7}a$.

- 23) M. Roger: Phys. Rev. B **30** (1984) 6432.
 24) Since the ‘‘charge gap’’ shows a linear V_{cutoff} dependence for large V_{cutoff} , we used small- V_{cutoff} data for the least-squares fit.
 25) A. F. Andreev and I. M. Lifshitz: Sov. Phys. JETP **29** (1969) 1107.
 26) $\omega = 0$ corresponds to $E = \mu$ in the notation of the inset of Fig. 5(a) for the hole-doped case.
 27) S. Sakai, Y. Motome, and M. Imada: unpublished (arXiv: 0809.0950v1).